2017 IEEE International Conference on Robotics and Automation (ICRA)
Singapore, May 29 - June 3, 2017

Design, Modeling, and Control of Pneumatic Artificial Muscles with Integrated Soft Sensing

Jonathan P. King*, Luis E. Valle*, Nishant Pol†, and Yong-Lae Park‡

***Abstract*— Presented are techniques for designing, modeling, and control of reliable pneumatic artificial muscle actuators with integrated low profile sensors for position feedback. The sensor is fabricated through a three-dimensional manufacturing process based on a modified lathe approach for controlling viscous and viscoelastic materials as well as on direct writing of liquid metal. Next, a new precision pneumatic muscle design and its integration with the sensor is illustrated. A theoretical model and experimental characterization of the muscle-sensor package are presented with high correlation and repeatability. Finally, a position feedback sliding mode controller is implemented with a position error of $<$0.9% of maximum muscle contraction.**

I. INTRODUCTION

Pneumatic artificial muscles (PAMs) are a promising alternative to other types of actuators in several robotic systems [1]–[3]. PAMs provide advantages in applications where the local area of actuation requires high energy density, no reflected inertia, low added inertia [4], and inherent compliance [4], [5]. Yet, the advantages of PAMs could be bottle-necked by lack of compact feedback mechanisms for force and length that are conformable to the muscles. Previously, there have been rigid methods for obtaining position feedback from PAMs. Encoders [3], [6], potentiometers [7], and halleffect sensors [8] are among the most commonly used. Force feedback has also been done by using strain gauge setups [3], and gauge pressure sensing [6]. However, these rigid methods add volume and sometimes undesired additional structures, which can limit degrees of freedom (DOFs) of the system that could be useful in certain applications such as physical therapy and rehabilitation [5].

Two-dimensional soft sensors have been designed for sensing displacement and pressure and have the potential to accommodate for these needs [5], [9]. Position feedback control has been demonstrated with these sensors with the advantage of relaxed form factors but with comparable results to rigid methods [5]. These sensors allow for less adverse effects to natural DOFs of the system. These work well for position sensing, conforming to some geometry of the system to be controlled, but they do not conform to the geometry of the source of actuation directly, which tend to be PAMs. Three-dimensional (3D) helical soft sensors have been manufactured as a package with Kevlar-fiber embedded PAMs [10]. Still, coil density and hence sensitivity, are limited by this manufacturing process, and the sensor remains coupled to this particular PAM.

No feedback control has yet been implemented for this type of package. Other monolithic sensors/actuators have been designed [11], but with difficult transferability to commonly used actuation methods.

Another type of self-contained sensing PAMs is to either braid or wrap a conductive wire (e.g. copper wire) on a McKibben-type PAM following the mesh pattern for measuring inductance change of the wire with contraction of the muscle [12], [13]. The integration of the sensing element with the muscle involves with manual processes and may cause manufacturing errors in this case.

We present a muscle-sensor package that exploits form factor from the actuation source with minimal extra volume. To achieve this, a new manufacturing method for 3D helical sensors was used in which coil density, length, and diameter of the sensor can be controlled. In addition, a theoretical model of the resistance to muscle length mapping is presented, which highly matches the experimental data. Sensors with coil densities of 14 coils/cm with a resistance range of of 11.4 to 22.4 Ω for a range of 25% contraction have been achieved. The sensor can be quickly integrated to any existing pneumatic muscle of cylindrical geometry.

A new manufacturing method for the PAM was used to decrease stress concentration and prolong life, while also increasing precision and integrability with robotic systems.

Finally, a stability analysis and implementation of position feedback control of the PAM-sensor package were achieved using sliding mode.

II. DESIGN

A. Sensor

Previously, a 3D helical soft sensor was manufactured through using multiple-layer casting and a low-friction thread for embedding a helical microchannel in an elastic bladder [10]. The low-friction thread would then be removed and a liquid conductor (e.g. eutectic gallium-indium, EGaIn [14]) would be injected in the channel. Some limiting factors of this process are: the diameter of the low-friction fiber, the angle limit for the fiber to be pulled out, and how thick

This work was supported in part by the National Institute for Health grant NHLBI 1R21HL126081-01. Any opinions, figures, and conclusions or recommendations expressed in this material are those of the authors and do not necessarily reflect the views of the National Institute for Health.

* Jonathan King and Luis Valle are with the Robotics Institute, Carnegie Mellon University, Pittsburgh, PA 15213 and Contributed Equally. {jking2,vallelu}@andrew.cmu.edu

† Nishant Pol is with the Department of Electrical and Computer Engineering, Carnegie Mellon University, Pittsburgh, PA 15213. npol@andrew.cmu.edu

‡ Yong-Lae Park is with the Robotics Institute, Carnegie Mellon University, Pittsburgh, PA 15213, and also with the Department of Mechanical and Aerospace Engineering, Seoul National University, Seoul 08826, Korea. ylpark@cs.cmu.edu

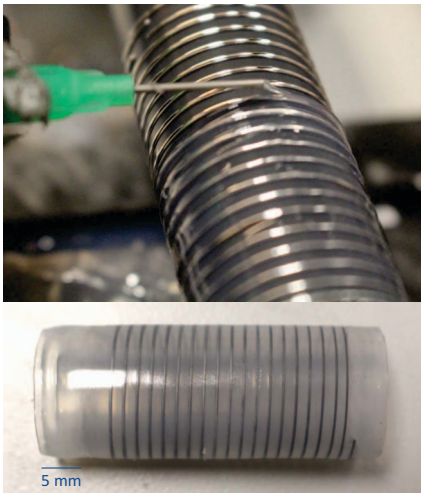

Fig. 1: Soft sensor fabrication image showing deposition of second polymer layer on EGaIn pattern (top) and complete prototype (bottom).

the polymer layer should be. Our sensor was designed to overcome some of these challenges. It is a hollow cylinder with an EGaIn[1] helical pattern as seen in Fig. 1 just like in the previous method. A modified mini-lathe[2] with two automated DOFs was used to manufacture the sensor. There is a three step process for the manufacturing process. First, silicone rubber[3] is poured on a rotating cylindrical surface and smoothed out with a smoothing tool, analogous with a cutting tool on a regular lathe. Then, a liquid metal high-density helical pattern is written on top of the cured silicone layer with a syringe pump[4]. The final step consists in adding another layer of silicone on the pattern while rotating, again with the syringe pump, in order to preserve the pattern. The process is controlled via a MATLAB program. The coil density, length, and diameter of the coil can be specified in the program. We fabricated two sensors for purposes of characterization. One sensor had 14 coils/cm and the other 9 coils/cm. The total length of both coils was about 2.54 cm. Because the PWM control is implemented on the solenoid valves, the isolated EGaIn sensors do not have any noticeable increase in temperature that affects the system.

B. Muscle

The implementation of PAMs has been, for the most part, divided into two camps. The first, containing the majority of PAM users, use very cheap and imprecise designs that allow for easy prototyping and concept testing. The other camp uses PAMs for precision applications in industry, requiring more reliable and accurate PAMs. The drawback of this approach is that there are few manufacturers, i.e. FESTO[5], with long lead-times and relatively high costs.

[1]Eutectic Gallium Indium, Alfa Aesar
[2]Sherline 4000, Sherline Products Inc
[3]Dragonskin 10, Smooth-On, Inc
[4]ERA-1000 Syringe Pump, Pump Systems Inc
[5] FESTO, Fluidic Muscle DMSP/MAS

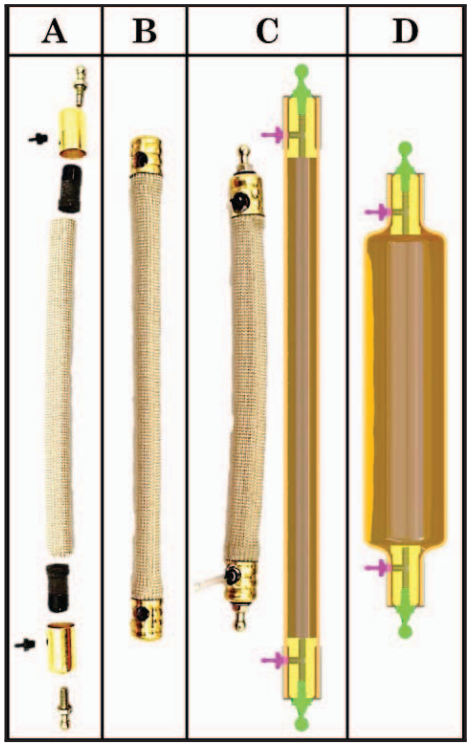

Fig. 2: PAM design and assembly detail: (A) Individual components; The muscle tube, inserts, ferrules, fittings and ball joints. (B) PAM after the inserts have been fit and the ferrules swaged and drilled. (C) Final PAM with fittings and ball joints & CAD cross-section for detail. (D) CAD cross-section of the inflated PAM.

The design method presented provides a cost-effective solution for increased PAM life-time, precision, and quality.

The PAM consists of an elastomeric bladder inside of an expandable braided sleeve. However, unlike most PAM designs, the bladder and sleeve are fabricated as a single unit. The ends replace the common zip tie seals with swaged brass ferrules and end-fittings that allow for a variety of air inlet options and mechanical interfacing such as rod ends and ball joints. The assembly and details of this design are shown in Fig. 2. For muscles utilizing the integrated sensor, the sensing device should be fitted over the muscle tube between steps A and B of the PAM assembly.

The result is a PAM that has higher pressure and force limits, improved fatigue life, precision mechanical interfacing, and repeatable manufacturing.

C. Circuit

An Arduino Uno[6] with an 8-bit microcontroller (Atmel ATmega328) was used to read sensor data and regulate PAM air pressure for closed-loop control. The sensor interface circuit shown in Fig. 3 drives the sense coil, R_{Sensor}, with a small fixed current. The Op Amp (Linear LT1077) maintains the preset reference voltage across R_{Set}, via

[6] Arduino Uno, Arduino

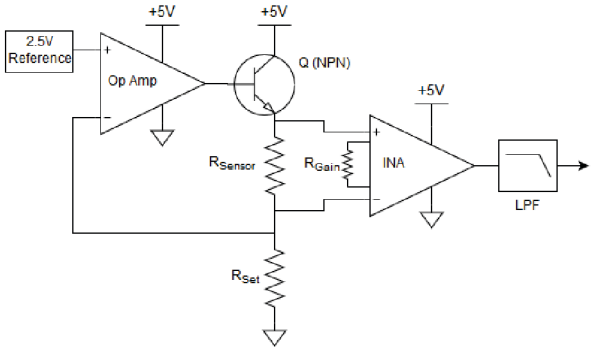

Fig. 3: Circuit used for feedback and actuation of the system.

transistor Q (2N3904). This fixes the current through R_{Set}, and R_{Sensor}. The Instrumentation Amplifier (INA, Analog Devices AD8226) amplifies the small voltage across R_{Sensor} to a range within the input limits of the microcontrollers ADC. A 1kHz single pole RC filter is used to prevent aliasing. The 2.5 V reference was implemented with a voltage divider.

III. MODELING

The braided fibers composing the PAM sheath and the EGaIn microchannel spanning the integrated sensor have a circular-helix shape. A helix can be defined by its axial-length (l), diameter (d), and number of coils (n), related by the arc-length (s) with the expression: $s^2 = l^2 + (\pi n d)^2$ (1). For the PAM, the fibers are assumed to be inextensible, leaving s_m and n_m constant. For a relative contraction of axial length, there will be a relative expansion in diameter. The strains, ϵ_{l_m} and ϵ_{d_m} are related by:

$$\begin{aligned}\epsilon_{d_m} &= \frac{\sqrt{s_m^2 - (\epsilon_{l_m} l_{m_i} + l_{m_i})^2}}{\pi n_m d_{m_i}} - 1 \\ &= \sqrt{1 - \alpha_m^2 \epsilon_{l_m}(2 + \epsilon_{l_m})/(\pi n_m)^2} - 1\end{aligned} \tag{2}$$

Where the measured initial values define the PAM aspect ratio, $\alpha_m = l_{m_i}/d_{m_i}$, and s_m is replaced using (1). Length and Diameter strains were measured and compared to the model with results in Fig. 4.

The expression for sensor resistance is: $R_s = \rho s_s / A_s$, where ρ is the EGain resistivity. The sensor design prevents slip along the PAM during contraction, thus the axial-length and diameter strains are equivalent for the PAM and sensor. Approximating the EGaIn fluid as incompressible we can define a constant volume given by the product of the channel arc-length and cross-sectional area, $V = s_s A_s$. This reduces the resistance expression to $R_s = \rho s_s^2 / V$. We can now relate the relative change in resistance from the initial measured state, $\epsilon_{R_s} = \Delta R_s / R_{s_i}$, to the PAM strain:

$$\begin{aligned}\epsilon_{R_s} &= \frac{\rho s_s^2 / V}{\rho s_{s_i}^2 / V} - 1 \\ &= \frac{(1+\epsilon_{l_m})^2 l_{s_i}^2 + (\pi n_s (1+\epsilon_{d_m}) d_{s_i})^2}{l_{s_i}^2 + (\pi n_s d_{s_i})^2} - 1\end{aligned} \tag{3}$$

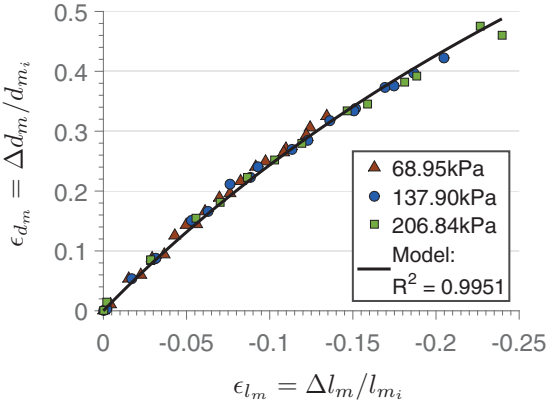

Fig. 4: Relative change in length vs. distance.

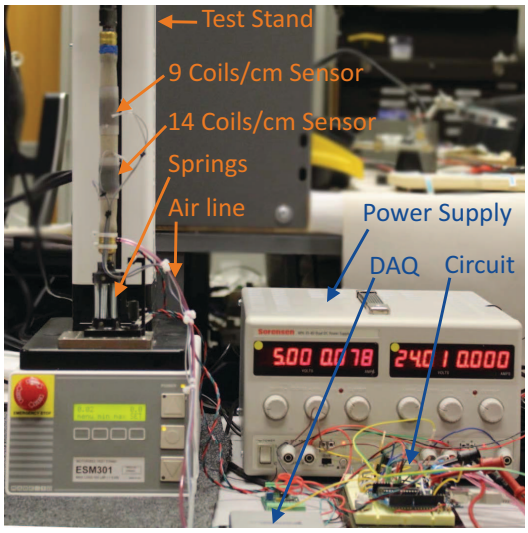

Fig. 5: Experimental setup for characterization of two sensors with muscle contraction.

Defining the sensor aspect ratio, $\alpha_s = l_{s_i}/d_{s_i}$, and the ratio of coils in the PAM and sensor helices, $\kappa_c = n_m/n_s$. Used together with (2), the resistance change reduces to:

$$\begin{aligned}\epsilon_{R_s} &= \underbrace{\frac{(\alpha_s \kappa_c)^2 - \alpha_m^2}{(\alpha_s \kappa_c)^2 + (\pi n_m)^2}}_{\text{constant} \rightarrow c_{sm}} \left(\epsilon_{l_m}^2 + 2\epsilon_{l_m}\right) \\ &= c_{sm}\epsilon_{l_m}(\epsilon_{l_m} + 2)\end{aligned} \tag{4}$$

Thus, the relative change in resistance is quadratically proportional to the relative change in the PAM length.

IV. CHARACTERIZATION

A. Experimental setup.

The experimental setup consists of a motorized test stand[7], air supply, a XPH 35-4D Dual DC Sorensen power supply, a microcontroller board (Arduino Uno), NI LABView 2010, a National Instruments DAQ, one PAM which ends are coupled

[7]Mark-10 Motorized Test Stand ESM301

to the test stand, a 14 coils/cm soft sensor, a 9 coils/cm soft sensor, and four 1.4 N/mm spring connected in parallel interfaced in series with the muscle, as shown in Fig. 5.

B. Procedure

First, the muscle was attached in series to the Mark-10 with a spring, and the sensors were connected with the specified circuit in Fig. 3. Then, the Mark-10 was setup to an initial length corresponding to the length of the muscle plus the length of the spring. After this, the muscle was connected to the air supply, and the following were measured: Load cell force F muscle length l_m, muscle diameter d_m, sensor 1 resistance R_{14}, sensor 2 resistance R_9, and gage pressure p_g. At this point, the Mark-10 was lowered, recording at least 10 readings total for each variable, until maximum contraction was reached. Data was also recorder while the Mark-10 was brought up until initial length of the muscle is reached, again, taking atleast 10 measurements for every variable.

The evaluated data is shown in Fig. 6. The correlation is very remarkable; a comparison of the model parameters from (4) with best-fit parameters in Table I effectively validates the characterization. It should be noted that because the measurements were taken for both loading and de-loading of the PAM, and little to no hysteresis was observed, that the sensor-length relationship is bidirectional. Thus, the sensor is a viable candidate for use in feedback control.

TABLE I: Characterization parameters.

	9 coils/cm		14 coils/cm	
	Theory	**Best**	**Theory**	**Best**
c_{sm}	-2.196	-2.165	-2.197	-2.165
R^2	0.993	0.994	0.998	0.998

Following characterization (4) can be restated with Δl_m as the dependent variable for implementation in the controller:

$$\Delta l_m(\Delta R_s) = l_{m_i}\left(\sqrt{\frac{\Delta R_s}{c_{sm}R_{s_i}}+1}-1\right) \tag{5}$$

V. CONTROL

An Arduino microcontroller[6] was used to control two valves[8] at 30 Hz for inflow and outflow of the PAM. Due to the high frequency response of the valves and lack of inertia, sliding mode was applied to the system.

A. Control Derivation

The following state space model was used to prove the stability of the system:

$$\dot{x}_1 = x_2 \tag{6a}$$
$$\dot{x}_2 = \frac{\bar{C}}{M}x_2 + \frac{\bar{K}}{M}x_1 \tag{6b}$$

Where x_1 and x_2 are position and velocity, with $\dot{x}_1$ and $\dot{x}_2$ are their time derivatives respectively. Position and velocity

[8]24V X-Valves, Parker Inc

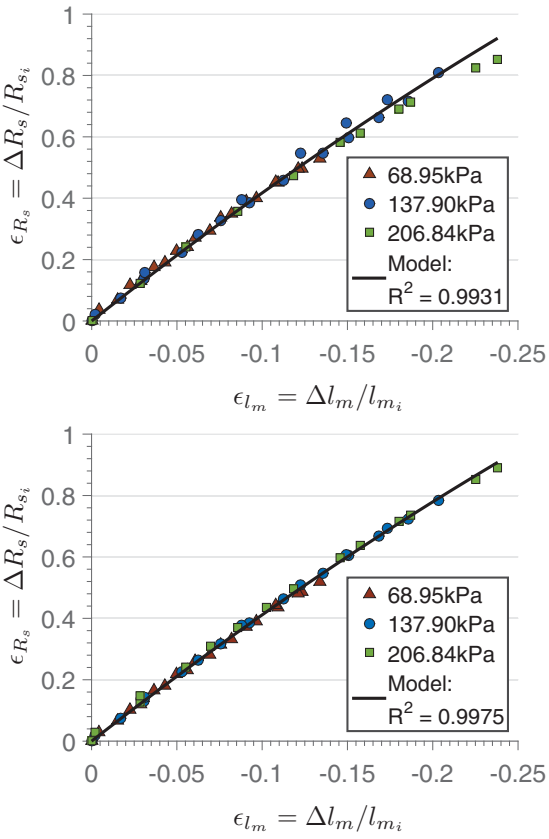

Fig. 6: Sensor characterization results showing relative change in length vs. resistance for 9 coils/cm (top) and 14 coils/cm (bottom).

are bounded: $\mathbf{x} \triangleq [x_1\ x_2]^T$, and $\mathbf{x} \in L_\infty$. $\bar{C}$ and $\bar{K}$ are upper bounds of the damping and spring coefficients of the system, and M is the total mass.

$$\frac{\bar{C}}{M}x_2 + \frac{\bar{K}}{M}x_1 = 0 \tag{7}$$

By solving (7), we arrive to (8a) and (8b), which shows that $\|\mathbf{x}\| \rightarrow 0$ as $t \rightarrow \infty$.

$$x_1(t) = x(0)e^{-\frac{\bar{K}}{\bar{C}}t} \tag{8a}$$
$$x_2(t) = -\frac{\bar{K}}{\bar{C}}x(0)e^{-\frac{\bar{K}}{\bar{C}}t} \tag{8b}$$

To improve the system's response convergence to stability and tracking, a low level digital controller is implemented. To do this, a control input is added to (6b), resulting in the state space of (9a) and (9b).

$$\dot{x}_1 = x_2 \tag{9a}$$
$$\dot{x}_2 = \frac{\bar{C}}{M}x_2 + \frac{\bar{K}}{M}x_1 + u \tag{9b}$$

We design the commonly used sliding manifold σ:

$$\sigma \triangleq \dot{e} + \alpha e; \quad \alpha \in \mathbb{R}_{>0} \tag{10}$$

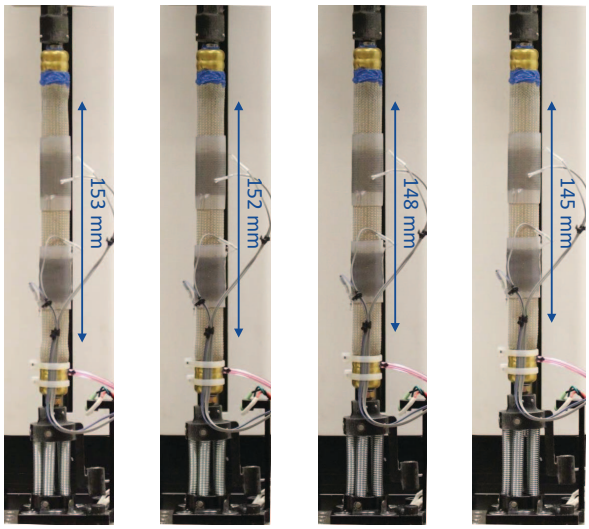

(a) (b) (c) (d)

Fig. 7: (a) Deflated PAM. (b) Inflated PAM at 69.0 kPa. (c) Inflated PAM at 137.9 kPa. (d) Inflated PAM at 206.8 kPa.

And design the control law, seen in (11).

$$u \triangleq K_s \text{sign}(\sigma) \tag{11}$$

where $K_s > 0$, and is a designed sliding mode gain.

Then, we do Lyapunov analysis to prove the stability of the controller, where we select positive definite lypunov function shown in (12).

$$V \triangleq \frac{1}{2}\sigma^2 \tag{12}$$

and its time derivative is found and simplified in (13).

$$\begin{aligned} \dot{V} &= \sigma \left(\underbrace{\frac{\bar{C}}{M}x_2 + \frac{\bar{K}}{M}x_1 + \frac{\bar{K}}{\bar{C}}x_2}_{W(x_1,x_2)} + u \right) \\ &= \sigma W(x_1, x_2) + \sigma \text{sign}(\sigma) \end{aligned} \tag{13}$$

We define constant $L \geq \|W(x_1, x_2)\|$. As we know the mass of the system, the upper limits of our stiffness and damping coefficients, and that x_1 and x_2 are bounded.

$$\text{sign}(\sigma) = \frac{|\sigma|}{\sigma} \tag{14}$$

We use (14) to upper bound the lyapunov. See (15).

$$\dot{V} \leq |\sigma| (L - K_s) \tag{15}$$

We assume that K_s will always dominate upper bound L. We will use positive variable $\bar{\beta}$ for simplicity. See (16).

$$\bar{\beta} \triangleq K_s - L \tag{16}$$

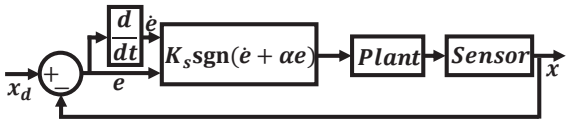

Fig. 8: Controller block diagram.

Using the sliding mode existence condition (17) from [15], which turns into (18), the asymptotic stability of the controller is proven. From this, our gain requirement (19) is selected. In so far as this gain requirement is satisfied and actuators used have infinite frequency, we can guarantee global asymptotic stability for our system. In practice, infinite frequency is not possible, but with high enough frequency response can be desirable.

$$\dot{V} \leq -\bar{\beta} V^{1/2} \tag{17}$$

$$\sigma\dot{\sigma} \leq -\frac{\bar{\beta}}{\sqrt{2}}|\sigma| \tag{18}$$

$$K_s = L + \frac{\bar{\beta}}{\sqrt{2}} \tag{19}$$

B. Control Results

The controller block diagram is shown in Fig. 8.

Since the characterization of both sensors were very similar, we only used the 14 coils/cm version for feedback. When experimenting with the control, α from (10) was set to a large value so it would dominate the velocity term. We did this to avoid the effects of the degrading signal of $\dot{e}$ due to the derivative. In future work, we will implement a nonlinear observer or output feedback in order to obtain a better response. Tracking control is shown to a reference point, a square wave, and a sinusoid in Figs. 9a, 9b, and 9c respectively. The rise time for our range was of at most 1.07 s, and the settling time was at most 0.2 s, with overshoot not larger than the ultimate bound.

VI. DISCUSSION

Figs. 4 and 6 show the comparison of measured data with models of how the muscle geometry and sensor resistance change. High coeffecients of determination, R^2, indicate that the models are accurate and that the sensor provides a force-independent measurement of muscle length.

Although asymptotic stability is shown in the analysis with (17), (18), the controller reaches an ultimate bound due to the limitations of our system. The computational limitation of arduino is the main factor that limits the frequency of our actuators. The other limitation is the resolution, which is restricted to 10-bit. Other than our limitations, sliding mode performs well in our system due to the inherent high frequency of the air valves used to inflate and deflate the muscle. The dynamics of the muscle are such that damping is also inherent in the system, so minimal overshoot and settling time are seen. The discrepancy of our sensor with the ground truth measurement was measured repeatedly. The discrepancy persists with negligible difference, meaning that

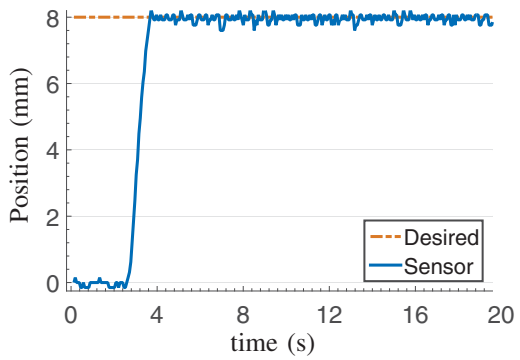

(a) Tracking control with 8 mm reference using 14 coils/cm sensor.

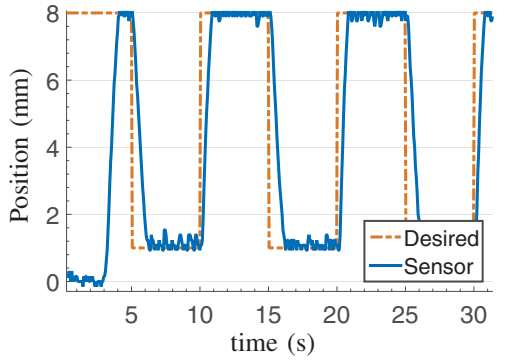

(b) Square-wave tracking using 14 coils/cm sensor.

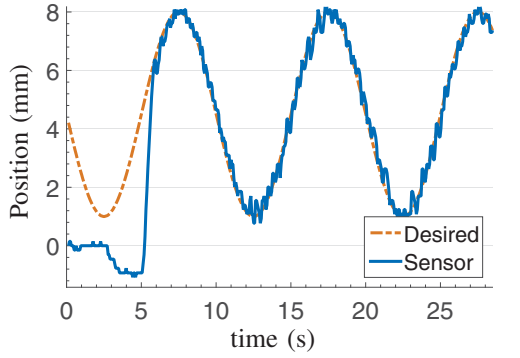

(c) Sinusoid tracking using 14 coils/cm sensor.

Fig. 9: Experimental control results.

calibration needs to be improved, but the sensor outputs repeatable values even under the influence of high frequency variations of air pressure.

VII. FUTURE WORK

In the future, a more detailed explanation of the manufacturing process will be presented. Currently, the materials selected were based on availability, a thorough investigation will be performed to choose more optimal materials. As new materials are implemented, detailed structural analysis will be performed to validate their use. A more robust method of interfacing with electrical connectors will be implemented to prevent potential leakage or damage of the EGaIn coils. Higher coil density will be pursued. Versatility of pattern writing during the manufacturing process will be shown. More extensive characterization of statics and dynamics of the system will be derived. A microcontroller with higher resolution and more computational power and possibly filtering will be used to improve performance. A force control method will be developed, with the goal of being robust to perturbations such as vibration and externally applied forces. The muscle-sensor package will be integrated to a robotic system for manipulation.

ACKNOWLEDGMENT

The authors would like to thank Yiwei Tao, Andrew Tallaksen, and Jin Zhu for their technical support.

REFERENCES

[1] G. Andrikopoulos, G. Nikolakopoulos, and S. Manesis, "A survey on applications of pneumatic artificial muscles," in *Control & Automation (MED), 2011 19th Mediterranean Conference on*. IEEE, 2011, pp. 1439–1446.

[2] F. Daerden and D. Lefeber, "Pneumatic artificial muscles: actuators for robotics and automation," *European journal of mechanical and environmental engineering*, vol. 47, no. 1, pp. 11–21, 2002.

[3] C.-P. Chou and B. Hannaford, "Measurement and modeling of mckibben pneumatic artificial muscles," *IEEE Transactions on robotics and automation*, vol. 12, no. 1, pp. 90–102, 1996.

[4] M. Wehner, B. Quinlivan, P. M. Aubin, E. Martinez-Villalpando, M. Baumann, L. Stirling, K. Holt, R. Wood, and C. Walsh, "A lightweight soft exosuit for gait assistance," in *Robotics and Automation (ICRA), 2013 IEEE International Conference on*. IEEE, 2013, pp. 3362–3369.

[5] Y.-L. Park, B.-r. Chen, N. O. Pérez-Arancibia, D. Young, L. Stirling, R. J. Wood, E. C. Goldfield, and R. Nagpal, "Design and control of a bio-inspired soft wearable robotic device for ankle–foot rehabilitation," *Bioinspiration & Biomimetics*, vol. 9, no. 1, p. 016007, 2014.

[6] A. Hildebrandt, O. Sawodny, R. Neumann, and A. Hartmann, "Cascaded control concept of a robot with two degrees of freedom driven by four artificial pneumatic muscle actuators," in *Proceedings of the 2005, American Control Conference, 2005.* IEEE, 2005, pp. 680–685.

[7] H. M. Herr and R. D. Kornbluh, "New horizons for orthotic and prosthetic technology: artificial muscle for ambulation," in *Smart structures and materials*. International Society for Optics and Photonics, 2004, pp. 1–9.

[8] D. Caldwell, G. Medrano-Cerda, and M. Goodwin, "Braided pneumatic actuator control of a multi-jointed manipulator," in *Systems, Man and Cybernetics, 1993.'Systems Engineering in the Service of Humans', Conference Proceedings., International Conference on*. IEEE, 1993, pp. 423–428.

[9] Y.-L. Park, B.-R. Chen, and R. J. Wood, "Design and fabrication of soft artificial skin using embedded microchannels and liquid conductors," *IEEE Sensors Journal*, vol. 12, no. 8, pp. 2711–2718, 2012.

[10] Y.-L. Park and R. J. Wood, "Smart pneumatic artificial muscle actuator with embedded microfluidic sensing," in *SENSORS, 2013 IEEE*. IEEE, 2013, pp. 1–4.

[11] R. A. Bilodeau, E. L. White, and R. K. Kramer, "Monolithic fabrication of sensors and actuators in a soft robotic gripper," in *Intelligent Robots and Systems (IROS), 2015 IEEE/RSJ International Conference on*. IEEE, 2015, pp. 2324–2329.

[12] W. Felt, K. Y. Chin, and C. D. Remy, "Contraction sensing with smart braid mckibben muscles," *IEEE/ASME Transactions on Mechatronics*, vol. 21, no. 3, pp. 1201–1209, June 2016.

[13] O. Erin, N. Pol, L. Valle, and Y.-L. Park, "Design of a bio-inspired pneumatic artificial muscle with self-contained sensing," in *The Engineering in Medicine and Biology Society (EMBC'16), 2016 IEEE International Conference of*. IEEE, 2016, pp. 2115–2119.

[14] M. D. Dickey, R. C. Chiechi, R. J. Larsen, E. A. Weiss, D. A. Weitz, and G. M. Whitesides, "Eutectic gallium-indium (EGaIn): A liquid metal alloy for the formation of stable structures in microchannels at room temperature," *Advanced Functional Materials*, vol. 18, no. 7, pp. 1097–1104, 2008.

[15] Y. Shtessel, C. Edwards, L. Fridman, and A. Levant, *Sliding mode control and observation*. Springer, 2014.